Atmos. Meas. Tech., 9, 2119–2134, 2016
www.atmos-meas-tech.net/9/2119/2016/
doi:10.5194/amt-9-2119-2016

Atmospheric Measurement Techniques Open Access EGU

Algorithm update of the GOSAT/TANSO-FTS thermal infrared CO_2 product (version 1) and validation of the UTLS CO_2 data using CONTRAIL measurements

Naoko Saitoh[1], Shuhei Kimoto[1], Ryo Sugimura[1], Ryoichi Imasu[2], Shuji Kawakami[3], Kei Shiomi[3], Akihiko Kuze[3], Toshinobu Machida[4], Yousuke Sawa[5], and Hidekazu Matsueda[5]

[1]Center for Environmental Remote Sensing, Chiba University, Chiba, Japan
[2]Atmosphere and Ocean Research Institute, University of Tokyo, Kashiwa, Japan
[3]Japan Aerospace Exploration Agency, Tsukuba, Japan
[4]National Institute for Environmental Studies, Tsukuba, Japan
[5]Meteorological Research Institute, Tsukuba, Japan

Correspondence to: Naoko Saitoh (nsaitoh@faculty.chiba-u.jp)

Received: 15 October 2015 – Published in Atmos. Meas. Tech. Discuss.: 10 December 2015
Revised: 27 April 2016 – Accepted: 27 April 2016 – Published: 13 May 2016

Abstract. The Thermal and Near Infrared Sensor for Carbon Observation (TANSO)–Fourier Transform Spectrometer (FTS) on board the Greenhouse Gases Observing Satellite (GOSAT) has been observing carbon dioxide (CO_2) concentrations in several atmospheric layers in the thermal infrared (TIR) band since its launch. This study compared TANSO-FTS TIR version 1 (V1) CO_2 data and CO_2 data obtained in the Comprehensive Observation Network for TRace gases by AIrLiner (CONTRAIL) project in the upper troposphere and lower stratosphere (UTLS), where the TIR band of TANSO-FTS is most sensitive to CO_2 concentrations, to validate the quality of the TIR V1 UTLS CO_2 data from 287 to 162 hPa. We first evaluated the impact of considering TIR CO_2 averaging kernel functions on CO_2 concentrations using CO_2 profile data obtained by the CONTRAIL Continuous CO_2 Measuring Equipment (CME), and found that the impact at around the CME level flight altitudes ($\sim$ 11 km) was on average less than 0.5 ppm at low latitudes and less than 1 ppm at middle and high latitudes. From a comparison made during flights between Tokyo and Sydney, the averages of the TIR upper-atmospheric CO_2 data were within 0.1 % of the averages of the CONTRAIL CME CO_2 data with and without TIR CO_2 averaging kernels for all seasons in the Southern Hemisphere. The results of comparisons for all of the eight airline routes showed that the agreements of TIR and CME CO_2 data were worse in spring and summer than in fall and winter in the Northern Hemisphere in the upper troposphere. While the differences between TIR and CME CO_2 data were on average within 1 ppm in fall and winter, TIR CO_2 data had a negative bias up to 2.4 ppm against CME CO_2 data with TIR CO_2 averaging kernels at the northern low and middle latitudes in spring and summer. The negative bias at the northern middle latitudes resulted in the maximum of TIR CO_2 concentrations being lower than that of CME CO_2 concentrations, which led to an underestimate of the amplitude of CO_2 seasonal variation.

1 Introduction

Carbon dioxide (CO_2) in the atmosphere is a well-known strong greenhouse gas (IPCC, 2013, and references therein), with concentrations that have been observed both in situ and by satellite sensors. Its long-term observation began in Mauna Loa, Hawaii, and the South Pole in the late 1950s (Keeling et al., 1976a, b, 1996). Since then, comprehensive CO_2 observations in the atmosphere have been conducted worldwide in several observatories and tall towers (Bakwin et al., 1998), by aircraft flask sampling (e.g., Crevoisier et al., 2010), and via the AirCore sampling system (Karion et al., 2010) in the framework of research by the National Oceanic and Atmospheric Administration (NOAA). Atmo-

spheric CO_2 concentrations have gradually increased at a globally averaged annual rate of 1.7 ± 0.5 ppm from 1998 to 2011, although its growth rate has relatively large interannual variation (IPCC, 2013). Upper-atmospheric CO_2 observations have been made in many areas by several projects using commercial airliners, such as the Comprehensive Observation Network for TRace gases by AIrLiner (CONTRAIL) project (Machida et al., 2008) and the Civil Aircraft for the Regular Investigation of the atmosphere Based on an Instrument Container (CARIBIC) project (Brenninkmeijer et al., 2007). Continuous long-term measurements of CO_2 made by several airplanes of Japan Airlines (JAL) in the CONTRAIL project have revealed details of its seasonal variation and interhemispheric transport in the upper atmosphere (Sawa et al., 2012) and interannual and long-term trends of its latitudinal gradients (Matsueda et al., 2015).

Atmospheric CO_2 observations by satellite sensors are categorized into two types: those utilizing CO_2 absorption bands in the shortwave infrared (SWIR) regions at around 1.6 and 2.0 µm, and those in the thermal infrared (TIR) regions at around 4.6, 10, and 15 µm. The Scanning Imaging Absorption Spectrometer for Atmospheric Chartography (SCIAMACHY) on the Environmental Satellite (ENVISAT) first observed CO_2 column-averaged dry-air mole fractions (XCO_2) from spectra at 1.57 µm (Buchwitz et al., 2005; Barkley et al., 2006). The Thermal and Near Infrared Sensor for Carbon Observation (TANSO)–Fourier Transform Spectrometer (FTS) on board the Greenhouse Gases Observing Satellite (GOSAT), which was launched in 2009 (Yokota et al., 2009), has observed XCO_2 with high precision by utilizing the 1.6 and/or 2.0 µm CO_2 absorption bands (Yoshida et al., 2011, 2013; O'Dell et al., 2012; Butz et al., 2011; Cogan et al., 2012). The Orbiting Carbon Observatory 2 (OCO-2) was successfully launched in 2014 and started regular observations of XCO_2 with high spatial resolution. Satellite CO_2 observations at TIR absorption bands have a longer history beginning with the High-Resolution Infrared Sounder (HIRS) (Chédin et al., 2002, 2003, 2005). The Atmospheric Infrared Sounder (AIRS) has achieved more accurate observations of middle- and upper-tropospheric CO_2 concentrations (Crevoisier et al., 2004; Chahine et al., 2005; Maddy et al., 2008; Strow and Hannon, 2008). The Tropospheric Emission Spectrometer (TES) has observed CO_2 concentrations in several vertical layers with high accuracy by taking advantage of its high wavelength resolution (Kulawik et al., 2010, 2013). The Infrared Atmospheric Sounding Interferometer (IASI) has observed upper-atmospheric CO_2 amounts from its TIR spectra (Crevoisier et al., 2009). TANSO-FTS also has a TIR band in addition to its three SWIR bands, and it obtains vertical information of CO_2 concentrations in addition to XCO_2 in the same field of view (Saitoh et al., 2009).

Rayner and O'Brien (2001) and Pak and Prather (2001) showed the utility of global CO_2 data obtained by satellite sensors for estimating its source and sink strength, and many studies of CO_2 inversion have been conducted using a huge amount of satellite data since the 2000s. Chevallier et al. (2005) first used satellite CO_2 data, observed with the Operational Vertical Sounder (TOVS), to estimate CO_2 surface fluxes. They reported that a regional bias in satellite CO_2 data hampers the outcomes. Nassar et al. (2011) demonstrated that the wide spatial coverage of satellite CO_2 data is beneficial to CO_2 surface flux inversion through the combined use of TES and surface flask CO_2 data, particularly in regions where surface measurements are sparse. In addition to CO_2 surface inversion results using TIR observations, global XCO_2 data observed with the SWIR bands of TANSO-FTS have been actively used for estimating CO_2 source and sink strength (Maksyutov et al., 2013; Saeki et al., 2013a; Chevallier et al., 2014; Basu et al., 2013, 2014; Takagi et al., 2014). One of the important things to consider when incorporating satellite data in CO_2 inversion is the accuracy of the data, as suggested by Basu et al. (2013). Uncertainties in satellite CO_2 data should be assessed seasonally and regionally to determine the seasonal and regional characteristics of the satellite CO_2 bias.

The importance of upper-atmospheric CO_2 data in the inversion analysis of CO_2 surface fluxes was discussed in Niwa et al. (2012). They used CONTRAIL CO_2 data in conjunction with surface CO_2 data to estimate surface flux, and they demonstrated that adding middle- and upper-tropospheric data observed by the aircraft could greatly reduce the posteriori flux errors, particularly in tropical Asian regions. Middle- and upper-tropospheric and lower-stratospheric CO_2 concentrations and column amounts of CO_2 can be simultaneously observed in the same field of view with TANSO-FTS on board GOSAT. Provided that the quality of upper-atmospheric CO_2 data simultaneously obtained with TANSO-FTS is proven to be comparable to that of TANSO-FTS XCO_2 data (Yoshida et al., 2013; Inoue et al., 2013), the combined use of upper-atmospheric CO_2 and XCO_2 data observed with TANSO-FTS could be a useful tool for estimating CO_2 surface flux.

GOSAT, which is the first satellite to be dedicated to greenhouse gas monitoring, was launched on 23 January 2009. As described above, TANSO-FTS on board GOSAT has been observing CO_2 concentrations in several vertical layers in the TIR band. In this study, we focused on CO_2 concentrations in the upper troposphere and lower stratosphere (UTLS), where the TIR band of TANSO-FTS is most sensitive. We validated these data by comparison with upper-atmospheric CO_2 data obtained in a wide spatial coverage in the CONTRAIL project. Sections 2 and 3 explain the GOSAT and CONTRAIL measurements, respectively. Section 4 details the retrieval algorithm used in the latest version 1 (V1) CO_2 level 2 (L2) product of the TIR band of TANSO-FTS. Section 5 describes the methods of comparing TANSO-FTS TIR V1 L2 and CONTRAIL CO_2 data. Sections 6 and 7 show and discuss the results of the comparisons between TIR and CONTRAIL CO_2 data. Section 8 summarizes this study.

2 GOSAT observations

GOSAT is a joint satellite project of the National Institute for Environmental Studies (NIES), Ministry of the Environment (MOE), and Japan Aerospace Exploration Agency (JAXA) for the purpose of making global observations of greenhouse gases such as CO_2 and CH_4 (Hamazaki et al., 2005; Yokota et al., 2009). It was launched on 23 January 2009, from the Tanegashima Space Center, and has continued its observations for more than 6 years. GOSAT is equipped with TANSO-FTS for greenhouse gas monitoring and the TANSO-Cloud and Aerosol Imager (CAI) to detect clouds and aerosols in the TANSO-FTS field of view (Kuze et al., 2009). TANSO-FTS consists of three bands in the SWIR region and one band in the TIR region. Column amounts of greenhouse gases are observed in the SWIR bands, and vertical information of gas concentrations are obtained in the TIR band (Yoshida et al., 2011, 2013; Saitoh et al., 2009, 2012; Ohyama et al., 2012, 2013).

Kuze et al. (2012) provided a detailed description of the methods used for the processing and calibration of level 1B (L1B) spectral data from TANSO-FTS. They explained the algorithm for the version 150.151 (V150.151) L1B spectral data. The TIR V1 L2 CO_2 product we focused on in this study was created from a later version, V161.160, of L1B spectral data. The following modifications were made to the algorithm from V150.151 to V161.160: improving the TIR radiometric calibration through the improvement of calibration parameters, turning off the sampling interval non-uniformity correction, modifying the spike noise criteria of the quality flag, and reevaluating the misalignment between the GOSAT satellite and TANSO-FTS sensor. Kataoka et al. (2014) reported that the biases of TANSO-FTS TIR V130.130 L1B radiance spectra based on comparisons with the Scanning High-resolution Interferometer Sounder (S-HIS) spectra for warm scenes were 0.5 K at 800–900 and 700–750 cm^{-1}, 0.1 K at 980–1080 cm^{-1}, and more than 2 K at 650–700 cm^{-1}. Although the magnitude of the spectral bias evaluated on the basis of V130.130 L1B data would change in V161.160 L1B data, the issue of L1B spectral bias still remains. The spectral bias inherent in TIR L1B spectra would be mainly because of uncertainty of polarization correction. Another possible cause was discussed in Imasu et al. (2010). When retrieving CO_2 concentrations from the TIR band of TANSO-FTS, the spectral bias that is predominant in CO_2 absorption bands should be considered (Ohyama et al., 2013).

3 CONTRAIL Continuous Measurement Equipment (CME) observations

We used CO_2 data obtained in the CONTRAIL project to validate the quality of TANSO-FTS TIR V1 L2 CO_2 data. CONTRAIL is a project to observe atmospheric trace gases such as CO_2 and CH_4 using instruments installed on commercial aircraft operated by JAL. Observations of trace gases in this project began in 2005. Two types of measurement instruments, the Automatic Air Sampling Equipment (ASE) and the Continuous CO_2 Measuring Equipment (CME), have been installed on several JAL aircraft to measure trace gases over a wide area (Machida et al., 2008).

This study used CO_2 data obtained with CME on several airline routes from Narita Airport, Japan. CO_2 observations with CME use a LI-COR LI-840 instrument that utilizes a nondispersive infrared absorption (NDIR) method (Machida et al., 2008). In the observations, two different standard gases, with CO_2 concentration of 340 and 390 ppm based on NIES09 scale, are regularly introduced into the NDIR for calibration. The accuracy of CME CO_2 measurements is 0.2 ppm. See Machida et al. (2008, 2011) and Matsueda et al. (2008) for details of the CME CO_2 observations and their accuracy and precision.

4 Retrieval algorithm of TANSO-FTS TIR V1 CO_2 data

4.1 Basic retrieval settings

Saitoh et al. (2009) provided an algorithm for retrieving CO_2 concentrations from the TIR band of TANSO-FTS. The first version, V00.01, of the L2 CO_2 product of the TIR band of TANSO-FTS was basically processed by the algorithm described in Saitoh et al. (2009). The V1 L2 CO_2 product that we focused on in this study also adopted a nonlinear maximum a posteriori (MAP) method with linear mapping, as was the case for the V00.01 product. We utilized the following expressions in TIR CO_2 retrieval:

$$\begin{aligned}\hat{\boldsymbol{z}}_{i+1} &= \mathbf{W}^{*}\boldsymbol{x}_{\mathrm{a}} + \mathbf{G}\left[\boldsymbol{y}\text{-}\boldsymbol{F}(\hat{\boldsymbol{x}}_i) + \mathbf{K}_i\mathbf{W}(\mathbf{W}^{*}\hat{\boldsymbol{x}}_i\text{-}\mathbf{W}^{*}\boldsymbol{x}_{\mathrm{a}})\right] \\ \mathbf{G} &= \left[\mathbf{W}^{\mathrm{T}}\mathbf{K}_i^{\mathrm{T}}\mathbf{S}_{\varepsilon}^{-1}\mathbf{K}_i\mathbf{W} + (\mathbf{W}^{*}\mathbf{S}_{\mathrm{a}}\mathbf{W}^{*\mathrm{T}})^{-1}\right]^{-1}\mathbf{W}^{\mathrm{T}}\mathbf{K}_i^{\mathrm{T}}\mathbf{S}_{\varepsilon}^{-1},\end{aligned} \quad (1)$$

where $\boldsymbol{x}_{\mathrm{a}}$ is an a priori vector, $\mathbf{S}_{\mathrm{a}}$ is a covariance matrix of the a priori vector, $\mathbf{S}_{\varepsilon}$ is a covariance matrix of measurement noise, $\mathbf{K}_{\mathrm{i}}$ is a CO_2 Jacobian matrix calculated using the ith retrieval vector $\hat{\boldsymbol{x}}_i$ on full grids, $\boldsymbol{F}(\hat{\boldsymbol{x}}_i)$ is a forward spectrum vector based on $\hat{\boldsymbol{x}}_i$, $\boldsymbol{y}$ is a measurement spectrum vector, and $\hat{\boldsymbol{z}}_{i+1}$ is the $i+1$th retrieval vector defined on retrieval grids. $\mathbf{W}$ is a matrix that interpolates from retrieval grids onto full grids. $\mathbf{W}^{*}$ is the generalized inverse matrix of $\mathbf{W}$.

The full grids are vertical layer grids for radiative transfer calculation, and the retrieval grids are defined as a subset of the full grids. In the V1 L2 CO_2 retrieval algorithm, linear mapping between retrieval grids and full grids was also applied, but the number of full grid levels was 78 instead of 110 in the V00.01 algorithm. The determination of retrieval grids in the V1 algorithm basically followed the method of the V00.01 algorithm. It was based on the areas of a CO_2 averaging kernel matrix in the tropics, but the retrieval grid levels were fixed for all of the retrieval processing, as presented in Table 1. Averaging kernel matrix $\mathbf{A}$ is defined (Rodgers,

Table 1. Retrieval grid layers of GOSAT/TANSO-FTS TIR CO_2 V1 data.

Layer level	Lower presure level (hPa)	Upper pressure level (hPa)
1	1165.91	857.70
2	857.70	735.64
3	735.64	630.96
4	630.96	541.17
5	541.17	464.16
6	464.16	398.11
7	398.11	341.45
8	341.45	287.30
9	287.30	237.14
10	237.14	195.73
11	195.73	161.56
12	161.56	133.35
13	133.35	110.07
14	110.07	90.85
15	90.85	74.99
16	74.99	61.90
17	61.90	51.09
18	51.09	42.17
19	42.17	34.81
20	34.81	28.73
21	28.73	23.71
22	23.71	19.57
23	19.57	16.16
24	16.16	13.34
25	13.34	10.00
26	10.00	5.62
27	5.62	1.00
28	1.00	0.10

2000) as

$$\mathbf{A} = \mathbf{GKW}. \quad (2)$$

Figure 1 shows typical averaging kernel functions of TIR V1 L2 CO_2 retrieval. The degrees of freedom (DF) in these cases (trace of the matrix **A**) were (a) 2.22, (b) 1.81, and (c) 1.36. The seasonally averaged DF values of TIR V1 CO_2 data ranged from 1.12 to 2.35. At the low and middle latitudes between 35° N and 35° S, the CO_2 DF values were around 2.0 or more; this means that observations by the TIR band of TANSO-FTS can provide information on CO_2 concentrations in more than two vertical layers, one of which we focused on in this study.

A priori and initial values for CO_2 concentrations were taken from the outputs of the NIES transport model (NIES-TM05) (Saeki et al., 2013b). A priori and initial values for temperature and water vapor were obtained from Japan Meteorological Agency (JMA) Grid Point Value (GPV) data. Basically, the retrieval processing of TANSO-FTS was only conducted under clear-sky conditions, which was judged based on a cloud flag from TANSO-CAI in the daytime (Ishida and Nakajima, 2009; Ishida et al., 2011) and on a TANSO-FTS TIR spectrum in the nighttime.

4.2 Improvements in the TIR V1 CO_2 algorithm

The following conditions are the improvements made in the TANSO-FTS TIR V1 L2 CO_2 algorithm from the V00.01 algorithm. The V1 algorithm used the CO_2 10 μm absorption band in addition to the CO_2 absorption band at around the 15 μm band; the wavelength regions of 690–750, 790–795, 930–990, and 1040–1090 cm^{-1} were used in the CO_2 retrieval. We did not apply any channel selection. In these wavelength regions, temperature, water vapor, and ozone concentrations were retrieved simultaneously with CO_2 concentration. Moreover, surface temperature and surface emissivity were simultaneously derived as a correction parameter of the spectral bias inherent in TANSO-FTS TIR V161.160 L1B spectra at the above-mentioned CO_2 absorption bands. We assumed that the spectral bias could be divided into two components: a wavelength-dependent bias whose amount varied depending on wavelength and a wavelength-independent bias whose amount was uniform in a certain wavelength region. We tried to correct such a wavelength-independent component of the spectral bias by adjusting the value of surface temperature. Similarly, a wavelength-dependent component of the spectral bias was corrected by adjusting the value of surface emissivity in each wavelength channel. Therefore the matrices of **K** and $\mathbf{S}_a$ of expression (1) are as follows:

$$\mathbf{K} = \left(\mathbf{K}_{CO_2}\mathbf{K}_{H_2O}\mathbf{K}_{O_3}\mathbf{K}_T\boldsymbol{k}_{sT\_1}\boldsymbol{k}_{sT\_2}\boldsymbol{k}_{sT\_3}\boldsymbol{k}_{sT\_4}\boldsymbol{k}_{sT\_5}\right.$$
$$\left.\boldsymbol{k}_{sE\_1}\boldsymbol{k}_{sE\_2}\boldsymbol{k}_{sE\_3}\boldsymbol{k}_{sE\_4}\boldsymbol{k}_{sE\_5}\right), \quad (3)$$

$$\mathbf{S}_a = \begin{vmatrix} \mathbf{S}_{CO_2} & & & & & & & & & & & & & & \\ & \mathbf{S}_{H_2O} & & & & & & & & & & & & & \\ & & \mathbf{S}_{O_3} & & & & & & & & & & & & \\ & & & \mathbf{S}_T & & & & & & & & & & & \\ & & & & S_{sT\_1} & & & & & & & & & & \\ & & & & & S_{sT\_2} & & & & & & & & & \\ & & & & & & S_{sT\_3} & & & & & & & & \\ & & & & & & & S_{sT\_4} & & & & & & & \\ & & & & & & & & S_{sT\_5} & & & & & & \\ & & & & & & & & & S_{sE\_1} & & & & & \\ & & & & & & & & & & S_{sE\_2} & & & & \\ & & & & & & & & & & & S_{sE\_3} & & & \\ & & & & & & & & & & & & S_{sE\_4} & & \\ & & & & & & & & & & & & & S_{sE\_5} & \end{vmatrix}, \quad (4)$$

where $\mathbf{K}_{CO_2}$, $\mathbf{K}_{H_2O}$, $\mathbf{K}_{O_3}$, and $\mathbf{K}_T$ are Jacobian matrices of CO_2, water vapor, ozone, and temperature on full grids, respectively, and $\mathbf{S}_{CO_2}$, $\mathbf{S}_{H_2O}$, $\mathbf{S}_{O_3}$, and $\mathbf{S}_T$ are a priori covariance matrices of CO_2, water vapor, ozone, and temperature on full grids, respectively. The vectors $\boldsymbol{k}_{sT\_1}$, $\boldsymbol{k}_{sT\_2}$, $\boldsymbol{k}_{sT\_3}$, $\boldsymbol{k}_{sT\_4}$, and $\boldsymbol{k}_{sT\_5}$ are the Jacobian vectors of surface temperature in the wavelength regions of 690–715, 715–750, 790–795, 930–990, and 1040–1090 cm^{-1}, respectively. The vectors $\boldsymbol{k}_{sE\_1}$, $\boldsymbol{k}_{sE\_2}$, $\boldsymbol{k}_{sE\_3}$, $\boldsymbol{k}_{sE\_4}$, and $\boldsymbol{k}_{sE\_5}$ are the Jacobian

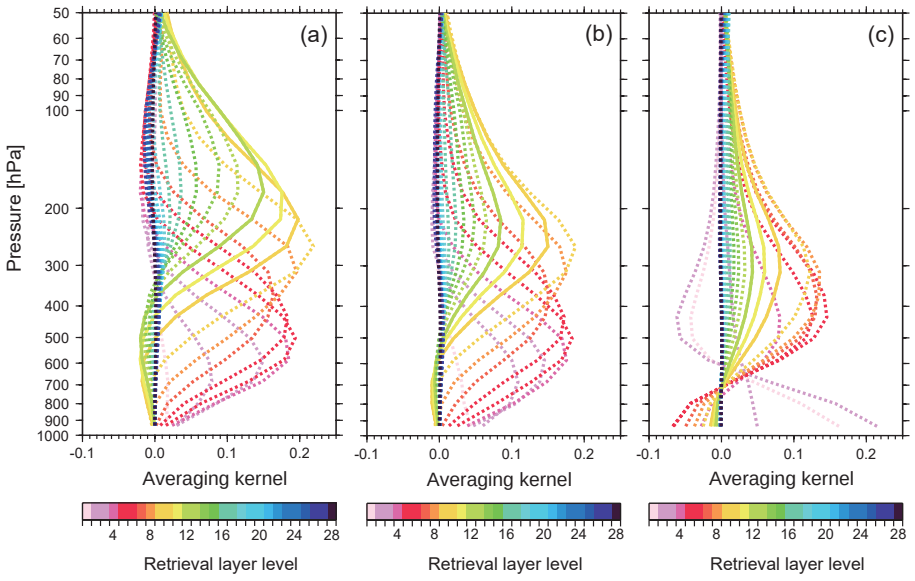

Figure 1. Averaging kernel functions of GOSAT/TANSO-FTS TIR V1 CO_2 retrieval in the 28 retrieval grid layers shown in Table 1: **(a)** low latitudes in summer, **(b)** middle latitudes in spring, and **(c)** high latitudes in winter. Solid orange, yellow, and green lines indicate averaging kernel functions of each of the three layer levels: 9, 10, and 11, respectively.

vectors of surface emissivity in each of the five wavelength regions. The elements of the Jacobian vectors of surface parameters that were defined for each of the five wavelength regions were set to be zero in the other wavelength regions. The values S_{sT_1}, S_{sT_2}, S_{sT_3}, S_{sT_4}, and S_{sT_5} and S_{sE_1}, S_{sE_2}, S_{sE_3}, S_{sE_4}, and S_{sE_5} are a priori variances of surface temperature and surface emissivity in each of the five wavelength regions, respectively. Simultaneous retrieval of the surface parameters in the V1 algorithm was conducted just for the purpose of correcting the TIR V161.160 L1B spectral bias; it had no physical meaning. We estimated the surface parameters separately in each of the five wavelength regions to consider differences in the amount of spectral bias in each wavelength region. The matrices $\mathbf{S}_a$ for CO_2, temperature, water vapor, and ozone were diagonal matrices with vertically fixed diagonal elements with a standard deviation of 2.5 %, 3 K, 20 %, and 30 %, respectively. Here, a priori and initial values for ozone were obtained from the climatological data for each latitude bin for each month given by MacPeters et al. (2007). We assumed rather large values as a priori variances of the surface parameters (a standard deviation of 10 K for surface temperature), which could allow more flexibility in the L1B spectral bias correction by the surface parameters. The a priori and initial values for surface emissivity were calculated by linear regression analysis using the Advanced Space-borne Thermal Emission Reflection Radiometer (ASTER) Spectral Library (Baldridge et al., 2009) using land-cover classification, vegetation, and wind speed information. The a priori and initial values for surface temperature were estimated using radiance data in several channels around 900 cm^{-1} of the TIR V161.160 L1B spectra.

In the TIR V1 L2 algorithm, we estimated surface temperature and surface emissivity to correct the spectral bias inherent in the TANSO-FTS TIR L1B spectra (Kataoka et al., 2014). The existence of a relatively large spectral bias around the CO_2 15 µm absorption band in TANSO-FTS TIR L1B spectra (Kataoka et al., 2014) resulted in a decrease in the number of normally retrieved CO_2 profiles. This is probably because the TIR L1B spectral bias in the CO_2 15 µm absorption band was sometimes too large for the L2 retrieval calculation to converse in a limited iteration. The correction of the TIR L1B spectral bias through the simultaneous retrieval of the surface parameters did not affect retrieved CO_2 concentrations in the UTLS regions, which was the focus of this study, but it altered the number of normally retrieved CO_2 profiles. The correction of the TIR L1B spectral bias through the simultaneous retrieval of surface temperature increased the number of normally retrieved CO_2 profiles. This implies that a wavelength-independent component of the spectral bias in CO_2 absorption bands could be reduced by adjusting the value of surface temperature at the bands. In contrast, the spectral bias correction through the simultaneous retrieval of surface emissivity did not increase the number of normally retrieved CO_2 profiles. If the TIR L1B spectral bias has a wavelength dependence, surface emissivity could be effective for correcting such a wavelength-dependent bias. A more effective method of L1B spectral bias correction based on surface emissivity should be considered in the next version of the TIR L2 CO_2 retrieval algorithm if a future version of the TIR L1B spectral data still has a bias.

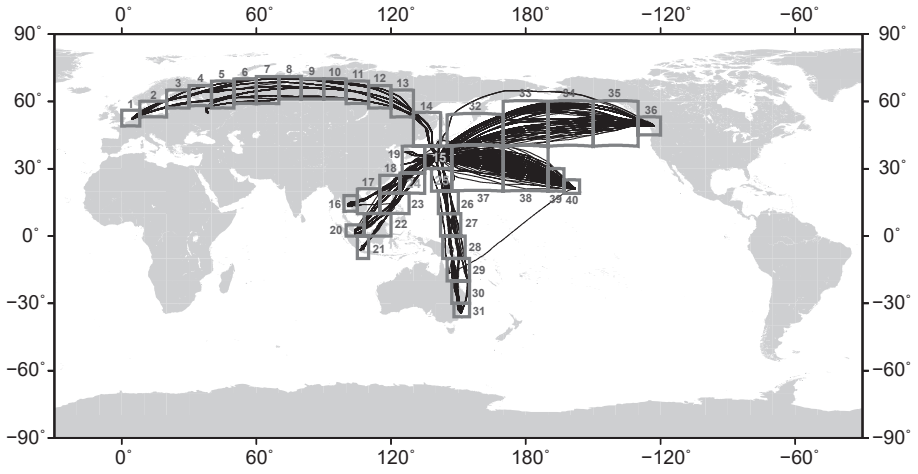

Figure 2. Flight tracks of all of the CONTRAIL CME observations in 2010 used in this study. The number next to each box area indicates its area number.

5 Comparison methods

5.1 Area comparisons

Here, we used the level flight CO_2 data of CONTRAIL CME observations in 2010 to validate the quality of UTLS CO_2 data from the TANSO-FTS TIR V1 L2 CO_2 product. The level flight data obtained from the following eight airline routes of the CONTRAIL CME observations were used in this study: Tokyo–Amsterdam (NRT–AMS) and Tokyo–Moscow (NRT–DME), Tokyo–Vancouver (NRT–VYR), Tokyo–Honolulu (NRT–HNL), Tokyo–Bangkok (NRT–BKK), Tokyo–Singapore (NRT–SIN) and Tokyo–Jakarta (NRT–CGK), and Tokyo–Sydney (NRT–SYD). We merged the level flight data of Tokyo–Amsterdam and Tokyo–Moscow into "Tokyo–Europe", and the data of Tokyo–Singapore and Tokyo–Jakarta into "Tokyo–East Asia". Figure 2 shows the flight tracks of all of the CONTRAIL CME observations in 2010 used in this study. As shown in the figure, we divided the CONTRAIL CME level flight data into 40 areas following Niwa et al. (2012), and compared them with TANSO-FTS TIR CO_2 data in each area in each season. The amount of level flight data varied depending on the area and season. The largest amount of data was obtained in area 15 over Narita Airport, where 4694–9306 data points were obtained. A relatively small amount of level flight data, 79–222 data points, was obtained in area 1 over Amsterdam. In all 40 areas, we collected sufficient level flight data to undertake comparison analysis based on the average values, except for seasons and regions with no flights.

5.2 Comparisons of CME profiles with and without averaging kernels

In comparisons of TIR V1 L2 CO_2 data with the CONTRAIL CME level flight data, it is difficult to smooth the CME data by applying TIR CO_2 averaging kernels, because CO_2 concentrations below and above the CME flight levels were not observed. Here, we evaluated the impact of considering averaging kernel functions on CO_2 concentrations using the CME profile data. We regarded the CME data obtained during the ascent and descent flights over the nine airports as part of CO_2 vertical profiles, and investigated differences between TIR and CME CO_2 data with and without applying averaging kernel functions in the altitude regions around the CME level flight observations. We assumed the CME ascending/descending CO_2 concentration at the uppermost altitude level to be constant up to the tropopause height, following the method proposed by Araki et al. (2010). We used stratospheric CO_2 data taken from the Nonhydrostatic Icosahedral Atmospheric Model (NICAM)–Transport Model (TM) (Niwa et al., 2011, 2012) to create whole CO_2 vertical profiles over the airports. The NICAM-TM CO_2 data used here introduced CONTRAIL CO_2 data to the inverse model in addition to surface CO_2 data, and therefore could simulate upper-atmospheric CO_2 concentrations well (Niwa et al., 2012). We determined the stratospheric CO_2 profile by assuming the CO_2 concentration gradients, calculated on the basis of the NICAM-TM CO_2 data above the tropopause height.

To compare these CME CO_2 profiles with TIR CO_2 data, we calculated a weighted average of all the CME CO_2 data included in each of the 28 retrieval grid layers with respect to altitude, and defined the CO_2 data in the 28 layers as "CONTRAIL (raw)" data. Then, we selected TIR CO_2 data that coincided with each of the CONTRAIL (raw) profiles. The criteria for the coincident pairs were a 300 km distance

from Narita airport, and a 3-day difference of each other observation. We applied TIR CO_2 averaging kernel functions to the corresponding CONTRAIL (raw) profile, as follows (Rodgers and Connor, 2003):

$$\boldsymbol{x}_{\text{CONTRAIL (AK)}} = \boldsymbol{x}_{\text{a priori}} + \mathbf{A}\left(\boldsymbol{x}_{\text{CONTRAIL (raw)}} - \boldsymbol{x}_{\text{a priori}}\right). \quad (5)$$

Here, $\boldsymbol{x}_{\text{CONTRAIL (raw)}}$ and $\boldsymbol{x}_{\text{a priori}}$ are CONTRAIL (raw) and a priori CO_2 profiles. We defined the CONTRAIL (raw) data with TIR CO_2 averaging kernel functions as "CONTRAIL (AK)" data.

5.3 Level flight comparisons

In this study, we made comparisons between TIR and CONTRAIL CME level flight CO_2 data in two ways. The first was a direct comparison with original CME CO_2 data, i.e., CONTRAIL (raw) data. The second was a comparison with CONTRAIL (AK) data in the altitude regions around the CME level flight observations that were based on "assumed CO_2 profiles" created at each of the measurement locations of all the CME level flight data. In the first comparison with CONTRAIL (raw) data, the CME level flight data in each of the 40 areas were averaged for each season (MAM, JJA, SON, and JF/DJF). The average altitude of all of the CME level flight data used here was 11.245 km. The airline routes of Tokyo–Europe, Tokyo–Vancouver, and Tokyo–Honolulu contained both tropospheric and stratospheric data in the areas along their routes; therefore, we calculated the average and standard deviation values separately. Here, we differentiated between the tropospheric and stratospheric level flight data on the basis of temperature lapse rates from the JMA GPV data that were interpolated to the CONTRAIL CME measurement locations. The average altitudes of the tropospheric and stratospheric level flight data from the airline route between Tokyo and Europe were 10.84 and 11.18 km, respectively.

In the comparison with CONTRAIL (raw) data, we selected TANSO-FTS TIR V1 L2 CO_2 data that were in the altitude range within ±1 km of the average altitude of the CME level flight data for each area for each season, and we calculated their averages and standard deviations. Similarly, we calculated the averages and standard deviations of the corresponding a priori CO_2 data for each area for each season. For the airline routes of Tokyo–Europe, Tokyo–Vancouver, and Tokyo–Honolulu, the averages and standard deviations of TIR V1 CO_2 data and the corresponding a priori CO_2 data were calculated separately for the tropospheric and stratospheric data. In this calculation, we first selected TIR V1 CO_2 data that were collected in a range within ±1 km of the average altitudes of the CONTRAIL tropospheric and stratospheric CO_2 data for each area. Then, we classified each of the selected TIR CO_2 data points into tropospheric and stratospheric data on the basis of the temperature lapse rates from the JMA GPV data that were interpolated to the TANSO-FTS measurement locations, and we calculated the seasonal averages and standard deviations for the reselected tropospheric and stratospheric TIR CO_2 data. This procedure was required for two reasons: (1) tropopause height at each TANSO-FTS measurement location should differ on a daily basis, and (2) because TIR CO_2 data were selected within the range of 2 km, some tropospheric TIR CO_2 data were selected on the basis of the CONTRAIL stratospheric level flight data, and vice versa. Figure 3 shows the number of TANSO-FTS TIR CO_2 data points that were finally selected in each retrieval layer for each of the airline routes. The TIR CO_2 data used in the comparative analysis were mainly from layers 9 and 10 (from 287 to 196 hPa) for the tropospheric comparison and from layers 10 and 11 (from 237 to 162 hPa) for the stratospheric comparison.

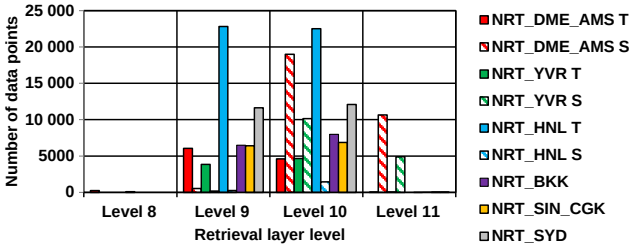

Figure 3. The number of GOSAT/TANSO-FTS TIR CO_2 data points compared to the CONTRAIL CME level flight data for each retrieval grid layer level for each flight. The numbers of TIR CO_2 data points in the troposphere ("T") and stratosphere ("S") are shown separately for the Tokyo–Europe (NRT_DME_AMS), Tokyo–Vancouver (NRT_YVR), and Tokyo–Honolulu (NRT_HNL) flight routes.

In the second comparison, we assumed a CO_2 vertical profile on the basis of CONTRAIL (raw) data at each of the CONTRAIL CME level flight locations and applied TIR CO_2 averaging kernel functions to the assumed profiles. For this purpose, realistic CO_2 vertical profiles were required along the eight airline routes. In this study, we created a CO_2 profile at each CME level flight measurement location from CarbonTracker CT2013B monthly-mean CO_2 data (Peters et al., 2007). The CarbonTracker CT2013B CO_2 data are available to the public, and therefore readers can refer to the data set that we used as a CO_2 climatological data set. The method for creating a CO_2 vertical profile from the CONTRAIL (raw) and CarbonTracker CT2013B data is as follows. We first averaged all of the CarbonTracker CT2013B monthly-mean data included in each of the 40 areas to create area-averaged CarbonTracker CT2013B profiles. Then, we shifted the area-averaged CarbonTracker CT2013B profile so that its concentration fit to each of the CONTRAIL (raw) data at CME level flight altitude. Finally, we applied area-averaged TIR CO_2 averaging kernel functions to each of the shifted area-averaged CO_2 profiles and created profiles of CONTRAIL (AK) at all the CME level flight measurement locations.

We compared the CONTRAIL (AK) data with TIR CO_2 data at the altitude regions around the CME level flight observations for each area in each season. We extracted CONTRAIL (AK) data that corresponded to the TIR retrieval layers where TIR CO_2 data were compared to CONTRAIL (raw) data, and we averaged them for each area for each season. For the airline routes of Tokyo–Europe, Tokyo–Vancouver, and Tokyo–Honolulu, we separately averaged CONTRAIL (AK) data created from tropospheric and stratospheric CONTRAIL (raw) data and defined the averages as tropospheric and stratospheric CONTRAIL (AK) data, respectively. As shown in Fig. 3, the CONTRAIL (AK) data used for the comparison during flights between Tokyo and Sydney consisted of CO_2 concentrations in layers 9 and 10 of the CONTRAIL (AK) profiles. For the flights between Tokyo and Europe, the CONTRAIL (AK) data used for the tropospheric and stratospheric comparisons were based on CO_2 concentrations in layers 9 and 10 and in layers 10 and 11 of CONTRAIL (AK) profiles, respectively.

6 Comparison results

6.1 Impacts of averaging kernels on CME profiles

Figure 4 shows comparisons of the differences between TANSO-FTS TIR and CONTRAIL (raw) CO_2 data, and the differences between TIR and CONTRAIL (AK) CO_2 data at low (BKK), middle (NRT and SYD), and high (DME) latitudes in layers 9, 10, and 11. At low latitudes, the differences between CONTRAIL (raw) and CONTRAIL (AK) were mostly less than 0.5 ppm in all seasons. This is because the tropopause heights there were much higher than the altitude levels of CONTRAIL CME level flight measurements, and CO_2 concentrations did not change much in the altitude regions where we compared TIR and CONTRAIL CME data. The same was true for other airports at low latitudes. While the differences between CONTRAIL (raw) and CONTRAIL (AK) were larger at middle and high latitudes than at low latitudes, they were in most cases less than 1 ppm in all seasons. In conclusion, the impact of applying the TIR CO_2 averaging kernels on CONTRAIL CME CO_2 data at around the CME level flight altitudes ($\sim$ 11 km) was on average less than 0.5 ppm at low latitudes and less than 1 ppm at middle and high latitudes.

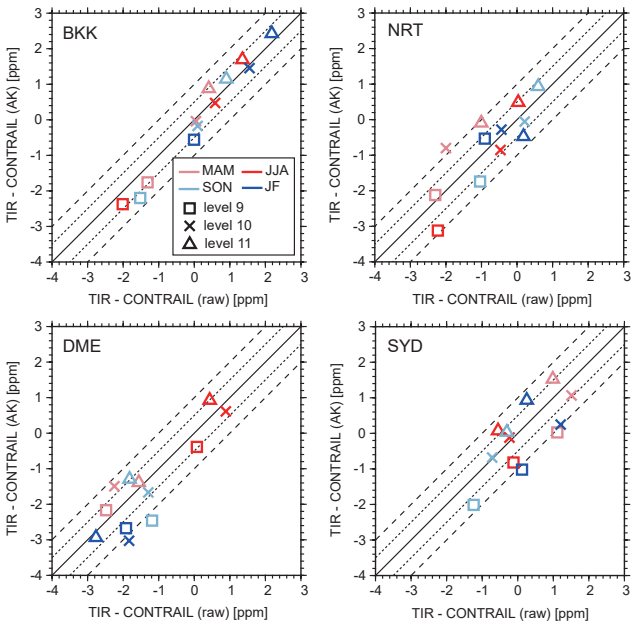

Figure 4. Scatterplots of GOSAT/TANSO-FTS TIR and CONTRAIL (raw) CO_2 differences and GOSAT/TANSO-FTS TIR and CONTRAIL (AK) CO_2 differences in layers 9, 10, and 11 for each season.

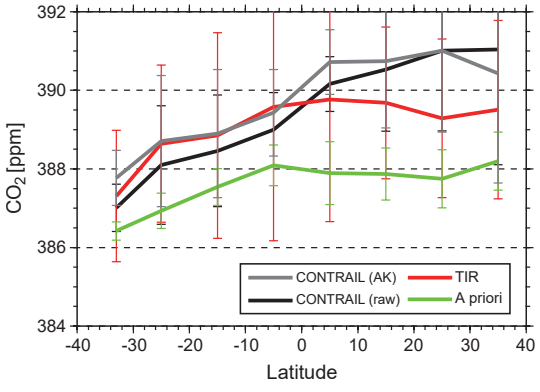

Figure 5. Comparisons among CONTRAIL (raw), CONTRAIL (AK), GOSAT/TANSO-FTS TIR, and a priori (NIES TM 05) CO_2 data during flights between Tokyo and Sydney (NRT_SYD) in northern hemispheric spring (MAM), shown by black, gray, red, and green lines, respectively. The means and their 1σ standard deviations were calculated in each area during the flight for all four data sets.

6.2 Comparisons during level flight

The airline route between Tokyo and Sydney covered a wide latitude range from the northern middle latitudes (35° N) to southern middle latitudes (34° S). Figure 5 shows comparisons among CONTRAIL (raw), CONTRAIL (AK), TANSO-FTS TIR, and a priori CO_2 data during flights between Tokyo and Sydney in northern hemispheric spring. In this case, we averaged CO_2 data mainly from layers 9 and 10 of the TIR retrieval layer levels. The 1σ values of the averages show the variability of CO_2 concentrations in these UTLS layers. The average of the TIR CO_2 data agreed better with the averages of the CONTRAIL (raw) and (AK) CO_2 data than the a priori CO_2 data at all latitudes. The differences between CONTRAIL (raw) and CONTRAIL (AK) were approximately 0.5 ppm, which is consistent with the result shown in Fig. 4, despite the fact that CONTRAIL (AK) data here were evaluated on the basis of CarbonTracker

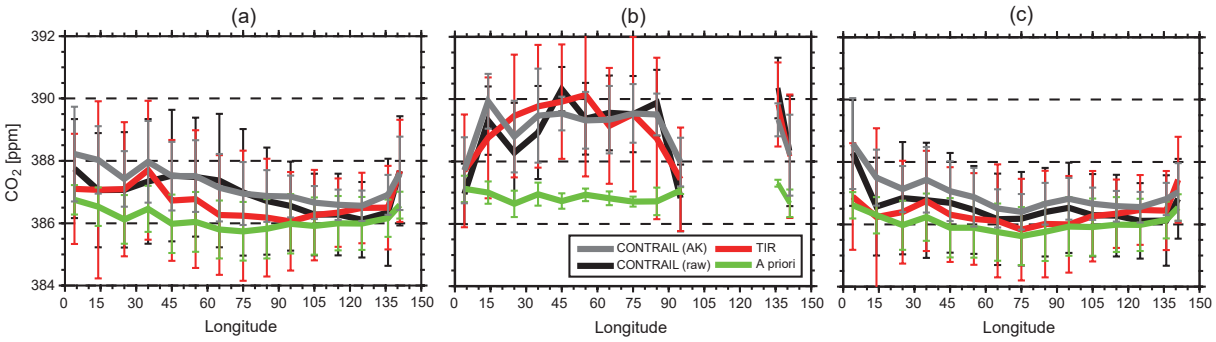

Figure 6. Same as Fig. 5 but for flights between Tokyo and Europe (NRT_DME_AMS) in winter (JF). **(a)** All of the data, **(b)** only data in the troposphere, and **(c)** only data in the stratosphere. See the text for the classification of tropospheric and stratospheric data.

monthly-mean data. In the Southern Hemisphere, the average of the TIR CO_2 data was within 0.1 % of the averages of the CONTRAIL (raw) and CONTRAIL (AK) CO_2 data. In the Northern Hemisphere, the average of the TIR CO_2 data agreed with the averages of the CONTRAIL (raw) and CONTRAIL (AK) CO_2 data to within 0.5 %, although the agreement was slightly worse there than in the Southern Hemisphere.

Along the airline route between Tokyo and Europe, both tropospheric and stratospheric CO_2 data were obtained in the CONTRAIL CME observations. Therefore, we were able to validate the quality of TANSO-FTS TIR CO_2 data for this route both in the upper troposphere and lower stratosphere using the UTLS CME CO_2 data. Here, we averaged CO_2 data mainly from layers 9 and 10 for the upper-tropospheric comparison and from layers 10 and 11 for the lower-stratospheric comparison. As shown in Fig. 6, the differences between CONTRAIL (raw) and CONTRAIL (AK) were again approximately 0.5 ppm when CONTRAIL CME data were divided into the upper troposphere and lower stratosphere, which is consistent with the result shown in Fig. 4. Figure 6b and c shows that the differences between the upper-tropospheric and lower-stratospheric CO_2 concentrations of CONTRAIL CME data were approximately 2–3 ppm in winter (maximum of 4.24 ppm in area 14). The upper-tropospheric and lower-stratospheric CO_2 concentrations from TANSO-FTS TIR V1 data also clearly differed, while the upper-tropospheric and lower-stratospheric CO_2 concentrations from a priori data were similar. The upper-tropospheric TIR CO_2 concentrations were in a good agreement within 1 ppm with the corresponding CONTRAIL (raw) and CONTRAIL (AK) data (Fig. 6b). In the lower stratosphere in winter (Fig. 6c), the averages of the CONTRAIL (raw), CONTRAIL (AK), TANSO-FTS TIR, and a priori CO_2 data were all within 0.5–1 ppm of each other.

Figure 7 shows the results of all of the comparisons among CONTRAIL (raw), CONTRAIL (AK), TANSO-FTS TIR, and a priori CO_2 data in the upper troposphere (left) and lower stratosphere (right) for each season. We divided the data for all four data sets in each of the 40 areas into six latitude bands: 40–20° S (areas 30 and 31), 20–0° S (areas 21, 28, and 29), 0–20° N (areas 16, 17, 20, 22, 23, 26, and 27), 20–40° N (areas 15, 18, 19, 24, 25, and 37–40), 40–60° N (areas 1, 2, 14, and 32–36), and 60–70° N (areas 3–13). As for the lower stratosphere, we showed the results at northern latitudes of 40° N where an adequate amount of data was obtained. Overall, the black and gray lines (TIR average minus CONTRAIL (raw) average, and TIR average minus CONTRAIL (AK) average) were closer to zero than the green lines (a priori average minus CONTRAIL (raw) average), which means that TIR CO_2 data agreed better with CONTRAIL CME CO_2 data than a priori CO_2 data.

The left panels of Fig. 7 show that the agreements between TIR and CONTRAIL (raw) and CONTRAIL (AK) CO_2 average data were worse in spring and summer than in fall and winter in the Northern Hemisphere in the upper troposphere. The differences between TIR and CONTRAIL (raw) and CONTRAIL (AK) CO_2 data were on average within 1 ppm in fall and winter in the northern troposphere. At 0–40° N in summer, in contrast, the TIR and a priori CO_2 average data were 2.3 ppm lower than the CONTRAIL (AK) CO_2 average data. At 20–40° N in spring, the differences between TIR and CONTRAIL (AK) CO_2 average data were 2.4 ppm, although the TIR CO_2 data had a better agreement with CONTRAIL CME CO_2 data than a priori CO_2 data. On the other hand, the averages of the TIR CO_2 data were within 0–0.7 ppm of the averages of the CONTRAIL (AK) CO_2 data in the Southern Hemisphere in all seasons, as in the comparison in northern hemispheric spring shown in Fig. 5.

In the lower stratosphere, the agreements between the average TANSO-FTS TIR and CONTRAIL CME CO_2 data did not have a smaller seasonality than in the upper troposphere. The averages of TIR and CONTRAIL (raw) and CONTRAIL (AK) CO_2 data agreed with each other within 0.5 % in all seasons.

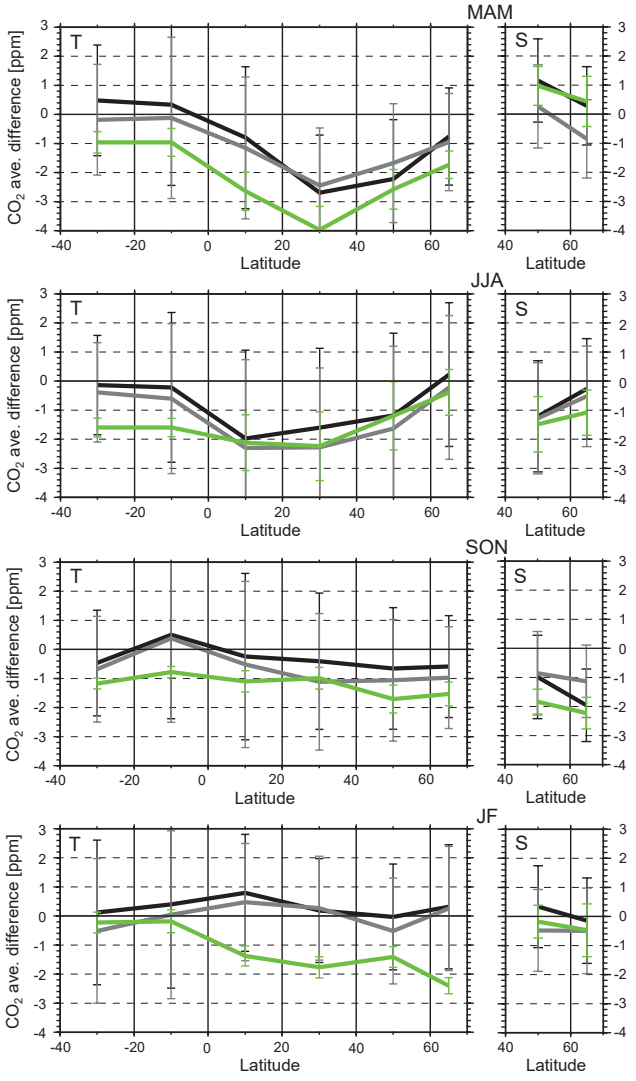

Figure 7. Differences between GOSAT/TANSO-FTS TIR and CONTRAIL (raw) averaged CO_2 data (TIR average minus CONTRAIL (raw) average), TIR and CONTRAIL (AK) averaged CO_2 data (TIR average minus CONTRAIL (AK) average), and a priori (NIES TM 05) and CONTRAIL (raw) averaged CO_2 data (a priori average minus CONTRAIL (raw) average) for each season for each latitude band (40–20° S, 20–0° S, 0–20° N, 20–40° N, 40–60° N, 60–70° N), shown by black, gray, and green lines, respectively. Left and right panels show the differences in the upper troposphere and lower stratosphere, respectively. The 1σ standard deviations of the latitudinal averages of TANSO-FTS TIR CO_2 data are shown by vertical bars.

7 Discussion

As shown in Fig. 7, TANSO-FTS TIR V1 L2 CO_2 data had a negative bias of 2.3–2.4 ppm against CONTRAIL CME CO_2 data at the northern low and middle latitudes in spring and summer. Uncertainties in surface parameters and temperature profiles could affect CO_2 retrieval in thermal infrared spectral regions. As described above, retrieving surface parameters simultaneously instead of using initial surface parameters did not affect CO_2 concentrations in the UTLS regions in the TIR V1 CO_2 retrieval. We compared simultaneously retrieved temperature profiles with a priori JMA GPV temperature profiles in the UTLS region and did not find any difference between the two which could explain the largest TIR CO_2 negative bias at the northern low and middle latitudes in spring and summer. In the UTLS regions, temperature variability is relatively large, and therefore comprehensive validation analysis of both the a priori and retrieved temperature profiles should be required using reliable and independent temperature data such as radiosonde data.

Uncertainty in a priori data could result in uncertainty in retrieved CO_2 data. Here, we arbitrarily decreased the a priori concentration by 1 % in a test TIR CO_2 retrieval and then compared the retrieved CO_2 concentrations with those retrieved using the original a priori data. At the northern low and middle latitudes in spring and summer where the DF values of TIR V1 CO_2 data were around 1.8 and more, a 1 % negative bias in a priori data could yield up to a 0.7 % negative bias in retrieved CO_2 concentrations in the altitude regions where we did comparisons between TIR and CONTRAIL CME data, although the magnitude of the bias varied depending on retrievals. As shown by the green lines in Figure 7, a priori CO_2 concentrations were underestimated by 2–4 ppm at the northern low and middle latitudes in spring and summer. The test TIR CO_2 retrieval demonstrated that the negative bias of a priori CO_2 data against CONTRAIL CME data is a possible cause of the TIR CO_2 negative bias in the UTLS regions at the northern low and middle latitudes in spring and summer.

In general, the information content of CO_2 observations made by TIR sensors is higher at middle and high latitudes in spring and summer than in fall and winter because of the thermal contrast in the atmosphere, with less seasonal dependence at low latitudes. Therefore, in spring and summer, retrieved CO_2 data contain more measurement information and are less constrained by a priori data at all latitudes. However, as shown in Fig. 7, the retrieved TIR CO_2 data at the northern low and middle latitudes did not sufficiently reduce the negative bias of the a priori CO_2 data in the UTLS regions in spring and summer. This implies the existence of factors that worsened CO_2 retrieval results other than the a priori data, especially in spring and summer. Another possible factor that worsened CO_2 retrieval results is the uncertainty in the calibration of TIR V161.160 L1B spectra. As reported in Kataoka et al. (2014), TANSO-FTS TIR V130.130 L1B radiance spectra had a wavelength-dependent bias ranging from 0.1 to 2 K. Although the characteristics of the spectral bias in V161.160 L1B data used in TIR V1 L2 CO_2 retrievals are still under investigation, we assumed the same degree of bias in V161.160 L1B spectra and evaluated the effect of the L1B spectral bias on the TIR CO_2 retrieval using the following

equation:

$$\boldsymbol{d}_{CO_2} = \mathbf{G}_{CO_2}\boldsymbol{d}_{spec}. \quad (6)$$

Here, $\mathbf{G}_{CO_2}$ is a gain matrix for CO_2 retrieval, $\boldsymbol{d}_{spec}$ is a spectral bias vector based on the evaluation by Kataoka et al. (2014), and $\boldsymbol{d}_{CO_2}$ is a vector of bias errors in retrieved CO_2 concentrations attributable to the spectral bias. The result showed that a wavelength-dependent bias comparable to V130.130 L1B spectra could yield up to 0.3 and 0.5 % uncertainties in retrieved CO_2 concentration in the UTLS regions at the northern middle latitude in spring and at the northern low latitude in summer, respectively. Uncertainty in the radiometric calibration of TANSO-FTS L1B spectra causes the spectral bias inherent in TIR L1B spectra. The temperatures of the internal blackbody on board the TANSO-FTS instrument partly reflect the environmental thermal conditions inside the instrument. The temperatures of FTS mechanics and aft optics on the optical bench of the TANSO-FTS instrument are precisely controlled at 23 °C. The difference in temperature between the environment inside the instrument and the optical bench could cause the uncertainty in the radiometric calibration of TANSO-FTS L1B spectra. Thus, the temperatures of the internal blackbody on board the TANSO-FTS instrument could be a parameter used to evaluate the TANSO-FTS TIR L1B spectral bias.

Figure 8 shows the averages of the partial degree of freedom of TANSO-FTS TIR V1 L2 CO_2 data for each of the areas along the airline routes between Tokyo and Europe in the upper troposphere (a) and the lower stratosphere (b) for each season. The partial DF is defined as the diagonal element of the averaging kernels corresponding to TIR CO_2 data that were compared to CONTRAIL CME level flight data, which is equal to the 9th, 10th, or 11th diagonal element of matrix **A**. As shown in Fig. 8, the average values of the partial DF of TIR lower-stratospheric CO_2 data were clearly lower than those of TIR upper-tropospheric CO_2 data for all of the fights between Tokyo and Europe. TIR upper-tropospheric CO_2 data were from layers 9 and 10, and TIR lower-stratospheric CO_2 data were from layers 10 and 11, as shown in Fig. 3, which led to a clear difference in partial DF values between the TIR upper-tropospheric and lower-stratospheric CO_2 data. The partial DF values of TIR upper-tropospheric CO_2 data were 0.13–0.20 in all of the areas for all seasons. In contrast, the partial DF values of TIR lower-stratospheric CO_2 data in spring, fall, and winter were ~ 0.05 in almost all of the areas, although they were as high as 0.1–0.14 in summer. From the results shown in Figs. 6c and 8, we conclude that TIR CO_2 retrieval results in the lower stratosphere in winter were constrained to the relatively good a priori CO_2 data due to the low information content and consequently had a good agreement with CONTRAIL CME CO_2 data. The comparisons in the areas during the airline route between Tokyo and Europe were included in the comparison results of 60–70° N in the right panels of Fig. 7. In this

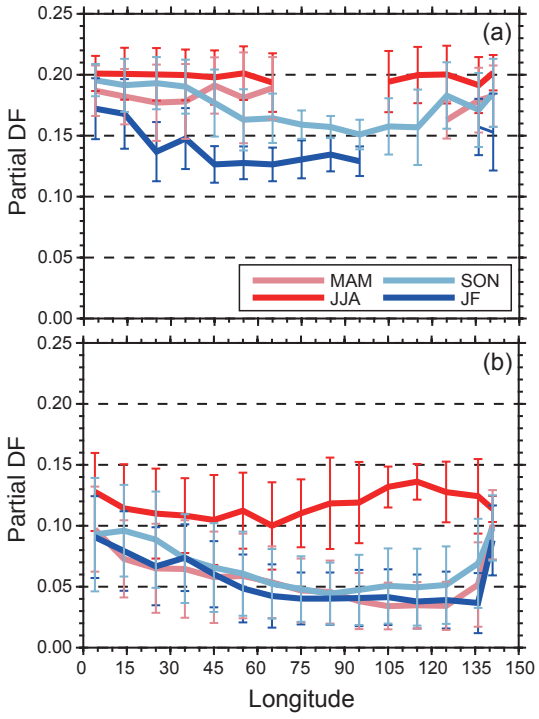

Figure 8. Partial degree of freedom (DF) for GOSAT/TANSO-FTS TIR CO_2 data in the upper troposphere **(a)** and the lower stratosphere **(b)** for each area of the flight between Tokyo and Europe (NRT_DME_AMS). The means and their 1σ standard deviations of the partial DF data were calculated in spring (MAM), summer (JJA), fall (SON), and winter (JF), as shown by the pink, red, light blue, and blue lines, respectively.

region, the average differences between a priori and CONTRAIL (raw) data were 1–2 ppm in summer and fall, while they were less than 0.5 ppm in spring and winter. In summer, TIR CO_2 retrievals had a relatively high information content compared to the other seasons, which led to an agreement between TIR and CONTRAIL (raw) and CONTRAIL (AK) CO_2 data of within 0.5 ppm. In fall, TIR CO_2 retrieval results in the lower stratosphere were more constrained to the a priori CO_2 data and therefore had a negative bias of approximately 1–2 ppm against CONTRAIL (raw) and CONTRAIL (AK) CO_2 data. In conclusion, the quality of TIR V1 CO_2 data in the lower stratosphere depends largely on the information content compared to the upper troposphere. In the case of high-latitude measurements, TIR V1 lower-stratospheric CO_2 data are only valid in summer.

We investigated the differences between TIR and CONTRAIL CO_2 comparison results in layers 9–11 with and without applying averaging kernel functions over the nine airports where CO_2 vertical profiles were observed during ascent and descent. At the northern middle latitudes in spring (NRT in Fig. 4), CONTRAIL (AK) was on average 0.2 and 1.2 ppm lower than CONTRAIL (raw) in layers 9 and 10. In contrast, the tendency was the opposite at the southern mid-

Table 2. Bias values of GOSAT/TANSO-FTS TIR V1 CO_2 data against CONTRAIL (AK) CO_2 data for each season and each latitude region in the upper troposphere and lower stratosphere in units of parts per million (ppm). Significant bias values larger than ±2 ppm are indicated by boldface.

UT LS	MAM		JJA		SON		JF	
60–70° N	−1.0	−0.8	−0.2	−0.5	−1.0	−1.1	0.3	−0.5
40–60° N	−1.7	0.3	−1.6	−1.3	−1.1	−0.9	−0.5	−0.5
20–40° N	**−2.4**		**−2.3**		−1.1		0.3	
0–20° N	−1.2		**−2.3**		−0.5		0.5	
20–0° S	−0.1		−0.6		0.4		0.0	
40–20° S	−0.2		−0.4		−0.7		−0.5	

dle latitudes in spring (SYD in Fig. 4); CONTRAIL (AK) was on average 1.1 and 0.4 ppm higher than CONTRAIL (raw) in layers 9 and 10. This means that CO_2 concentrations in layers 9 and 10 were more affected by stratospheric air with relatively low CO_2 concentrations at the northern middle latitude in spring, when considering averaging kernels. This is consistent with the result of Sawa et al. (2012) showing that the difference between upper-tropospheric and lower-stratospheric CO_2 concentrations was larger in the Northern Hemisphere in spring.

Using CONTRAIL CME level flight observations that covered wide spatial areas allowed us to discuss the longitudinal differences in the characteristics of TIR UTLS CO_2 data. In the comparison results of the airline routes of Tokyo–Europe (Fig. 6) and Tokyo–Vancouver (not shown here), the magnitudes of the differences between TIR and CONTRAIL (raw) and (AK) CO_2 data did not have a clear longitudinal dependence. Table 2 summarizes the latitudinal dependence of the magnitudes of the differences between TIR and CONTRAIL (AK) CO_2 data. In the upper troposphere within 0–60° N, negative biases in TIR CO_2 data against CONTRAIL CME CO_2 data ranged from 1.2 to 2.4 ppm in spring and summer when applying averaging kernels to the assumed CME CO_2 profiles created based on CarbonTracker CT2013B monthly-mean profiles. It is the negative biases at the northern low and middle latitudes that we should in particular be concerned about when using TIR V1 L2 CO_2 data in any scientific analysis. In the upper troposphere at the northern middle latitudes, CO_2 concentrations reach the maximum from spring through early summer. The negative biases in TIR CO_2 data resulted in the maximum TIR CO_2 concentrations being lower than that of the CONTRAIL CME CO_2 concentrations, which led to an underestimate of the amplitude of the CO_2 seasonal variation when using TIR CO_2 data without taking their negative biases into account.

8 Summary

In this study, we conducted a comprehensive validation of the UTLS CO_2 concentrations from the GOSAT/TANSO-FTS TIR V1 L2 CO_2 product. The TIR V1 L2 CO_2 algorithm used both the CO_2 10 and 15 μm absorption bands (690–750, 790–795, 930–990, and 1040–1090 cm^{-1}) and simultaneously retrieved vertical profiles of CO_2, water vapor, ozone, and temperature in these wavelength regions. Because the TANSO-FTS TIR V161.160 L1B radiance data used in the TIR V1 L2 CO_2 retrieval had a spectral bias, we simultaneously derived surface temperature and surface emissivity in the same wavelength regions as a corrective parameter, other than temperature and gas profiles, to correct the spectral bias. The simultaneous retrieval of surface temperature greatly increased the number of normally retrieved CO_2 profiles.

To validate the quality of TIR V1 upper-atmospheric CO_2 data, we compared them with the level flight CO_2 data of CONTRAIL CME observations along the following airline routes in 2010: Tokyo–Europe (Amsterdam and Moscow), Tokyo–Vancouver, Tokyo–Honolulu, Tokyo–Bangkok, Tokyo–East Asia (Singapore and Jakarta), and Tokyo–Sydney. For the CONTRAIL data obtained during the northern high-latitude flights, we made comparisons among CONTRAIL, TIR, and a priori CO_2 data separately in the upper troposphere and in the lower stratosphere. The TIR upper-tropospheric and lower-stratospheric CO_2 data that were compared were mainly from layers 9 and 10 (287–196 hPa) and from layers 10 and 11 (237–162 hPa), respectively. In this study, we evaluated the impact of considering TIR CO_2 averaging kernel functions on CO_2 concentrations using the CME profile data over the nine airports; the impact at around the CME level flight altitudes (∼ 11 km) was on average less than 0.5 ppm at low latitudes and less than 1 ppm at middle and high latitudes.

In the Southern Hemisphere, the averages of TANSO-FTS TIR V1 upper-atmospheric CO_2 data were within 0.1 % of the averages of CONTRAIL CO_2 data with and without TIR CO_2 averaging kernels for all seasons, from the limited comparisons made during flights between Tokyo and Sydney, while TIR CO_2 data had a better agreement with CONTRAIL CO_2 data than a priori CO_2 data, with the agreement being on average within 0.5 % in the Northern Hemisphere. The northern high-latitude comparisons suggest that the quality of TIR lower-stratospheric CO_2 data depends largely on the information content. At high latitudes, TIR

lower-stratospheric CO_2 data are only valid in summer, when their information content is highest. Overall, the agreements of TIR and CONTRAIL CME CO_2 data were worse in spring and summer than in fall and winter in the Northern Hemisphere in the upper troposphere. TIR CO_2 data had a negative bias up to 2.4 ppm against CONTRAIL CO_2 data with TIR CO_2 averaging kernels at the northern low and middle latitudes in spring and summer. This is partly because of the larger negative bias in the a priori CO_2 data. The spectral bias inherent to TANSO-FTS TIR L1B radiance data could cause a negative bias in retrieved CO_2 concentrations, particularly in summer. TIR sensors can make more observations than SWIR sensors. When using the TIR UTLS CO_2 data, the seasonally and regionally dependent negative biases of the TIR V1 L2 CO_2 data presented here should be taken into account.

Data availability

GOSAT/TANSO-FTS TIR and a priori CO_2 data and TIR CO_2 averaging kernel data are provided at http://www.gosat.nies.go.jp/en/. Contact the CONTRAIL project (http://www.cger.nies.go.jp/contrail/index.html) to access the CONTRAIL CME CO_2 data. CarbonTracker CT2013B and updated results are provided at http://carbontracker.noaa.gov.

Acknowledgements. We thank all of the members of the GOSAT Science Team and their associates. We are also grateful to the engineers of Japan Airlines, the JAL Foundation, and JAMCO Tokyo for supporting the CONTRAIL project. We thank Y. Niwa for providing the outputs of NICAM-TM CO_2 simulations. We thank T. Saeki and S. Maksyutov for providing information on the a priori data set. CarbonTracker CT2013B results were provided by NOAA Earth System Research Laboratory (ESRL), Boulder, Colorado, USA, from the website at http://carbontracker.noaa.gov. This study was supported by the Green Network of Excellence (GRENE-ei) of the Ministry of Education, Culture, Sports, and Technology. This study was performed within the framework of the GOSAT Research Announcement.

Edited by: H. Worden

References

Araki, M., Morino, I., Machida, T., Sawa, Y., Matsueda, H., Ohyama, H., Yokota, T., and Uchino, O.: CO_2 column-averaged volume mixing ratio derived over Tsukuba from measurements by commercial airlines, Atmos. Chem. Phys., 10, 7659–7667, doi:10.5194/acp-10-7659-2010, 2010.

Bakwin, P. S., Tans, P. P., Hurst, D. F., and Zhao, C.: Measurements of carbon dioxide on very tall towers: results of the NOAA/CMDL program, Tellus, 50B, 401–415, 1998.

Baldridge, A. M., Hook, S. J., Grove, C. I., and Rivera, G.: The ASTER spectral library version 2.0, Remote Sens. Environ., 113, 711–715, doi:10.1016/j.rse.2008.11.007, 2009.

Barkley, M. P., Frieß, U., and Monks, P. S.: Measuring atmospheric CO_2 from space using Full Spectral Initiation (FSI) WFM-DOAS, Atmos. Chem. Phys., 6, 3517–3534, doi:10.5194/acp-6-3517-2006, 2006.

Basu, S., Guerlet, S., Butz, A., Houweling, S., Hasekamp, O., Aben, I., Krummel, P., Steele, P., Langenfelds, R., Torn, M., Biraud, S., Stephens, B., Andrews, A., and Worthy, D.: Global CO_2 fluxes estimated from GOSAT retrievals of total column CO_2, Atmos. Chem. Phys., 13, 8695–8717, 2013.

Basu, S., Krol, M., Butz, A., Clerbaux, C., Sawa, Y., Machida, T., Matsueda, H., Frankenberg, C., Hasekamp, O. P., and Aben, I.: The seasonal variation of the CO_2 flux over Tropical Asia estimated from GOSAT, CONTRAIL, and IASI, Geophys. Res. Lett., 41, 1809–1815, 2014.

Brenninkmeijer, C. A. M., Crutzen, P., Boumard, F., Dauer, T., Dix, B., Ebinghaus, R., Filippi, D., Fischer, H., Franke, H., Frieß, U., Heintzenberg, J., Helleis, F., Hermann, M., Kock, H. H., Koeppel, C., Lelieveld, J., Leuenberger, M., Martinsson, B. G., Miemczyk, S., Moret, H. P., Nguyen, H. N., Nyfeler, P., Oram, D., O'Sullivan, D., Penkett, S., Platt, U., Pupek, M., Ramonet, M., Randa, B., Reichelt, M., Rhee, T. S., Rohwer, J., Rosenfeld, K., Scharffe, D., Schlager, H., Schumann, U., Slemr, F., Sprung, D., Stock, P., Thaler, R., Valentino, F., van Velthoven, P., Waibel, A., Wandel, A., Waschitschek, K., Wiedensohler, A., Xueref-Remy, I., Zahn, A., Zech, U., and Ziereis, H.: Civil Aircraft for the regular investigation of the atmosphere based on an instrumented container: The new CARIBIC system, Atmos. Chem. Phys., 7, 4953–4976, doi:10.5194/acp-7-4953-2007, 2007.

Buchwitz, M., de Beek, R., Burrows, J. P., Bovensmann, H., Warneke, T., Notholt, J., Meirink, J. F., Goede, A. P. H., Bergamaschi, P., Körner, S., Heimann, M., and Schulz, A.: Atmospheric methane and carbon dioxide from SCIAMACHY satellite data: initial comparison with chemistry and transport models, Atmos. Chem. Phys., 5, 941–962, doi:10.5194/acp-5-941-2005, 2005.

Butz, A., Guerlet, S., Hasekamp, O., Schepers, D., Galli, A., Aben, I., Frankenberg, C., Hartmann, J.-M., Tran, H., Kuze, A., Keppel-Aleks, G., Toon, G., Wunch, D., Wennberg, P., Deutscher, N., Griffith, D., Macatangay, R., Messerschmidt, J., Notholt, J., Warneke, T.: Toward accurate CO_2 and CH_4 observations from GOSAT, Geophys. Res. Lett., 38, L14812, doi:10.1029/2011GL047888, 2011.

Chahine, M., Barnet, C., Olsen, E. T., Chen, L., and Maddy, E.: On the determination of atmospheric minor gases by the method of vanishing partial derivatives with application to CO_2, Geophys. Res. Lett., 32, L22803, doi:10.1029/2005GL024165, 2005.

Chédin, A., Serrar, S., Armante, R., Scott, N. A., and Hollingsworth, A.: Signatures of annual and seasonal variations of CO_2 and other greenhouse gases from comparisons between NOAA TOVS observations and radiation model simulations, J. Climate, 15, 95–116, 2002.

Chédin, A., Serrar, S., Scott, N. A., Crevoisier, C., and Armante, R.: First global measurement of midtropospheric CO_2 from NOAA polar satellites, J. Geophys. Res., 108, 4581, doi:10.1029/2003JD003439, 2003.

Chédin, A., Serrar, S., Scott, N. A., Pierangelo, C., and Ciais, P.: Impact of tropical biomass burning emissions on the diurnal cycle of upper tropospheric CO_2 retrieved from NOAA 10 satellite observations, J. Geophys. Res., 110, D11309, doi:10.1029/2004JD005540, 2005.

Chevallier, F., Fisher, M., Peylin, P., Serrar, S., Bousquet, P., Bréon, F.-M., Chédin, A., and Ciais, P.: Inferring CO_2 sources and sinks from satellite observations: Method and application to TOVS data, J. Geophys. Res., 110, D24309, doi:10.1029/2005JD006390, 2005.

Chevallier, F., Palmer, P. I., Feng, L., Boesch, H., O'Dell, C. W., and Bousquet, P.: Toward robust and consistent regional CO_2 flux estimates from in situ and spaceborne measurements of atmospheric CO_2, Geophys. Res. Lett., 41, 1065–1070, 2014.

Climate Modeling and Diagnostics Laboratory (CMDL): Climate Modeling and Diagnostics Laboratory Summary Report No. 27 2002–2003, Boulder, Colorado, USA, 2004.

Cogan, A. J., Boesch, H., Parker, R. J., Feng, L., Palmer, P. I., Blavier, J.-F. L., Deutscher, N. M., Macatangay, R., Notholt, J., Roehl, C., Warneke, T., and Wunch, D.: Atmospheric carbon dioxide retrieved from the Greenhouse gases Observing SATellite (GOSAT): Comparison with ground-based TCCON observations and GEOS-Chem model calculations, J. Geophys. Res., 117, D21301, doi:10.1029/2012JD018087, 2012.

Comprehensive Observation Network for TRace gases by AIrLiner project: CONTRAIL project, available at: http://www.cger.nies.go.jp/contrail/index.html, last access: 15 October 2015.

Crevoisier, C., Heilliette, S., Chédin, A., Serrar, S., Armante, R., and Scott, N. A.: Midtropospheric CO_2 concentration retrieval from AIRS observations in the tropics, Geophys. Res. Lett., 31, L17106, doi:10.1029/2004GL020141, 2004.

Crevoisier, C., Chédin, A., Matsueda, H., Machida, T., Armante, R., and Scott, N. A.: First year of upper tropospheric integrated content of CO_2 from IASI hyperspectral infrared observations, Atmos. Chem. Phys., 9, 4797–4810, doi:10.5194/acp-9-4797-2009, 2009.

Crevoisier, C., Sweeney, C., Gloor, M., Sarmiento, J. L., and Tans, P. P.: Regional US carbon sinks from three-dimensional atmospheric CO_2 sampling, PNAS, 107, 18348–18353, 2010.

Greenhouse gases Observing SATellite project: GOSAT project, available at: http://www.gosat.nies.go.jp/en/, last access: 15 October 2015.

Hamazaki, T., Kaneko, Y., Kuze, A., and Kondo, K.: Fourier transform spectrometer for Greenhouse Gases Observing Satellite (GOSAT), P. Soc. Photo-Opt. Inst., 5659, 73–80, 2005.

Imasu, R., Hayashi, Y., Inagoya, A., Saitoh, N., and Shiomi, K.: Retrieval of minor constituents from thermal infrared spectra observed by GOSAT TANSO-FTS sensor, P. Soc. Photo-Opt. Inst., 7857, 785708, doi:10.1117/12.870684, 2010.

Inoue, M., Morino, I., Uchino, O., Miyamoto, Y., Yoshida, Y., Yokota, T., Machida, T., Sawa, Y., Matsueda, H., Sweeney, C., Tans, P. P., Andrews, A. E., Biraud, S. C., Tanaka, T., Kawakami, S., and Patra, P. K.: Validation of XCO_2 derived from SWIR spectra of GOSAT TANSO-FTS with aircraft measurement data, Atmos. Chem. Phys., 13, 9771–9788, doi:10.5194/acp-13-9771-2013, 2013.

Intergovernmental Panel on Climate Change (IPCC): Contribution of Working Group I to the Fifth Assessment Report of the Intergovernmental Panel on Climate Change, Cambridge University Press, Cambridge, UK and New York, NY, USA, 2013.

Ishida, H. and Nakajima, T. Y.: Development of an unbiased cloud detection algorithm for a spaceborne multispectral imager, J. Geophys. Res., 114, D07206, doi:10.1029/2008JD010710, 2009.

Ishida, H., Nakjima, T. Y., Yokota, T., Kikuchi, N., and Watanabe, H.: Investigation of GOSAT TANSO-CAI Cloud Screening Ability through an Intersatellite Comparison, J. Appl. Meteorol., 50, 1571–1586, 2011.

Karion, A., Sweeney, C., and Tans, P. P.; AirCore: An innovative atmospheric sampling system, J. Atmos. Ocean Tech., 27, 1839–1853, 2010.

Kataoka, F., Knuteson, R. O., Kuze, A., Suto, H., Shiomi, K., Harada, M., Garms, E. M., Roman, J. A., Tobin, D. C., Taylor, J. K., Revercomb, H. E., Sekio, N., Higuchi, R., and Mitomi, Y.: TIR spectral radiance calibration of the GOSAT satellite borne TANSO-FTS with the aircraft-based S-HIS and the ground-based S-AERI at the Railroad Valley desert playa, IEEE T. Geosci. Remote, 52, 89–105, 2014.

Keeling, C. D., Bacastow, R. B., Bainbridge, A. E., Ekdahl, C. A., Guenther, P. R., Waterman, L. S., and Chin, J. F. S.; Atmospheric carbon dioxide variations at Mauna Loa Observatory, Hawaii, Tellus, 28, 538–551, 1976a.

Keeling, C. D., Adams, J. A., Ekdahl, C. A., and Guenther, P. R.: Atmospheric carbon dioxide variations at the South Pole, Tellus, 28, 553–564, 1976b.

Keeling, C. D., Chin, J. F. S., and Whorf, T. P.: Increased activity of northern vegetation inferred from atmospheric CO_2 measurements, Nature, 382, 146–149, 1996.

Kulawik, S. S., Jones, D. B. A., Nassar, R., Irion, F. W., Worden, J. R., Bowman, K. W., Machida, T., Matsueda, H., Sawa, Y., Biraud, S. C., Fischer, M. L., and Jacobson, A. R.: Characterization of Tropospheric Emission Spectrometer (TES) CO_2 for carbon cycle science, Atmos. Chem. Phys., 10, 5601–5623, doi:10.5194/acp-10-5601-2010, 2010.

Kulawik, S. S., Worden, J. R., Wofsy, S. C., Biraud, S. C., Nassar, R., Jones, D. B. A., Olsen, E. T., Jimenez, R., Park, S., Santoni, G. W., Daube, B. C., Pittman, J. V., Stephens, B. B., Kort, E. A., Osterman, G. B., and TES team: Comparison of improved Aura Tropospheric Emission Spectrometer CO_2 with HIPPO and SGP aircraft profile measurements, Atmos. Chem. Phys., 13, 3205–3225, doi:10.5194/acp-13-3205-2013, 2013.

Kuze, A., Suto, H., Nakajima, M., and Hamazaki, T.: Thermal and near infrared sensor for carbon observation Fourier-transform spectrometer on the Greenhouse Gases Observing Satellite for greenhouse gases monitoring, Appl. Optics, 48, 6716–6733, 2009.

Kuze, A., Suto, H., Shiomi, K., Urabe, T., Nakajima, M., Yoshida, J., Kawashima, T., Yamamoto, Y., Kataoka, F., and Buijs, H.: Level 1 algorithms for TANSO on GOSAT: processing and on-orbit calibrations, Atmos. Meas. Tech., 5, 2447–2467, doi:10.5194/amt-5-2447-2012, 2012.

Machida, T., Matsueda, H., Sawa, Y., Nakagawa, Y., Hirotani, K., Kondo, N., Goto, K., Nakazawa, T., Ishikawa, K., and Ogawa, T.: Worldwide measurements of atmospheric CO_2 and other trace gas species using commercial airlines, J. Atmos. Ocean Tech., 25, 1744–1754, 2008.

Machida, T., Tohjima, Y., Katsumata, K., and Mukai, H.: A new CO_2 calibration scale based on gravimetric one-step dilution cylinders in National Institute for Environmental Studies – NIES 09 CO_2 Scale, 15th WMO/IAEA Meeting of Experts on Carbon Dioxide, Other Greenhouse Gases and Related Tracers Measurement Techniques, GAW Rep., 194, 165–169, World Meteorological Organization, Geneva, Switzerland, 2011.

Maddy, E. S., Barnet, C. D., Goldberg, M., Sweeney, C., and Liu, X.: CO_2 retrievals from the Atmospheric Infrared Sounder: Methodology and validation, J. Geophys. Res., 113, D11301, doi:10.1029/2007JD009402, 2008.

Maksyutov, S., Takagi, H., Valsala, V. K., Saito, M., Oda, T., Saeki, T., Belikov, D. A., Saito, R., Ito, A., Yoshida, Y., Morino, I., Uchino, O., Andres, R. J., and Yokota, T.: Regional CO_2 flux estimates for 2009–2010 based on GOSAT and ground-based CO2 observations, Atmos. Chem. Phys., 13, 9351–9373, doi:10.5194/acp-13-9351-2013, 2013.

Matsueda, H., Machida, T., Sawa, Y., Nakagawa, Y., Hirotani, K., Ikeda, H., Kondo, N., and Goto, K.: Evaluation of atmospheric CO_2 measurements from new flask air sampling of JAL airliner observations, Pap. Meteorol. Geophys., 59, 1–17, 2008.

Matsueda, H., Machida, T., Sawa, Y., and Niwa, Y.: Long-term change of CO_2 latitudinal distribution in the upper troposphere, Geophys. Res. Lett., 42, 2508–2514, 2015.

McPeters, R. D., Labow, G. J., and Logan, J. A.: Ozone climatological profiles for satellite retrieval algorithms, J. Geophys. Res., 112, D05308, doi:10.1029/2005JD006823, 2007.

Nassar, R., Jones, D. B. A., Kulawik, S. S., Worden, J. R., Bowman, K. W., Andres, R. J., Suntharalingam, P., Chen, J. M., Brenninkmeijer, C. A. M., Schuck, T. J., Conway, T. J., and Worthy, D. E.: Inverse modeling of CO_2 sources and sinks using satellite observations of CO_2 from TES and surface flask measurements, Atmos. Chem. Phys., 11, 6029–6047, doi:10.5194/acp-11-6029-2011, 2011.

Niwa, Y., Tomita, H., Satoh, M., and Imasu, R.: A threedimensional icosahedral grid advection scheme preserving monotonicity and consistency with continuity for atmospheric tracer transport, J. Meteorol. Soc. Jpn., 89, 255–268, 2011.

Niwa, Y., Machida, T., Sawa, Y., Matsueda, H., Schuck, T. J., Brenninkmeijer, C. A. M., Imasu, R., and Satoh, M.: Imposing strong constraints on tropical terrestrial CO_2 fluxes using passenger aircraft based measurements, J. Geophys. Res., 117, D11303, doi:10.1029/2012JD017474, 2012.

O'Dell, C. W., Connor, B., Bösch, H., O'Brien, D., Frankenberg, C., Castano, R., Christi, M., Crisp, D., Eldering, A., Fisher, B., Gunson, M., McDuffie, J., Miller, C. E., Natraj, V., Oyafuso, F., Polonsky, I., Smyth, M., Taylor, T., Toon, G. C., Wennberg, P. O., and Wunch, D.: Corrigendum to "The ACOS CO_2 retrieval algorithm – Part 1: Description and validation against synthetic observations" published in Atmos. Meas. Tech., 5, 99–121, 2012, Atmos. Meas. Tech., 5, 193–193, doi:10.5194/amt-5-193-2012, 2012.

Ohyama, H., Kawakami, S., Shiomi, K., and Miyagawa, K.: Retrievals of Total and Tropospheric Ozone From GOSAT Thermal Infrared Spectral Radiances, IEEE T. Geosci. Remote, 50, 1770–1784, 2012.

Ohyama, H., Kawakami, S., Shiomi, K., Morino, I., and Uchino, O.: Atmospheric Temperature and Water Vapor Retrievals from GOSAT Thermal Infrared Spectra and Initial Validation with Coincident Radiosonde Measurements, SOLA, 9, 143–147, 2013.

Pak, B. C. and Prather, M. J.: CO_2 sources inversions using satellite observations of the upper troposphere, Geophys. Res. Lett., 28, 4571–4574, 2001.

Peters, W., Jacobson, A. R., Sweeney, C., Andrews, A. E., Conway, T. J., Masarie, K., Miller, J. B., Bruhwiler, L. M. P., Petron, G., Hirsch, A. I., Worthy, D. E. J., van der Werf, G. R., Randerson, J. T., Wennberg, P. O., Krol, M. C., and Tans, P. P.: An atmospheric perspective on North American carbon dioxide exchange: CarbonTracker, PNAS, 48, 104, 18925–18930, available at: http://carbontracker.noaa.gov (last access 17 February 2016), 2007.

Rayner, P. J. and O'Brien, D. M.: The utility of remotely sensed CO_2 concentration data in surface source inversions, Geophys. Res. Lett., 28, 175–178, 2001.

Rodgers, C. D.: Inverse method for atmospheric sounding, World Scientific Publishing, Singapore, 2000.

Rodgers, C. D. and Connor, B. J.: Intercomparison of remote sounding instruments, J. Geophys. Res., 108, 4116, doi:10.1029/2002JD002299, 2003.

Saeki, T., Maksyutov, S., Saito, M., Valsala, V., Oda, T., Andres, R. J., Belikov, D., Tans, P., Dlugokencky, E., Yoshida, Y., Morino, I., Uchino, O., and Yokota, T.: Inverse Modeling of CO_2 Fluxes Using GOSAT Data and Multi-Year Ground-Based Observations, SOLA, 9, 45–50, 2013a.

Saeki, T., Saito, R., Belikov, D., and Maksyutov, S.: Global high-resolution simulations of CO_2 and CH_4 using a NIES transport model to produce a priori concentrations for use in satellite data retrievals, Geosci. Model Dev., 6, 81–100, doi:10.5194/gmd-6-81-2013, 2013b.

Saitoh, N., Imasu, R., Ota, Y., and Niwa, Y.: CO_2 retrieval algorithm for the thermal infrared spectra of the Greenhouse Gases Observing Satellite: potential of retrieving CO_2 vertical profile from high-resolution FTS sensor, J. Geophys. Res., 114, D17305, doi:10.1029/2008JD011500, 2009.

Saitoh, N., Touno, M., Hayashida, S., Imasu, R., Shiomi, K., Yokota, T., Yoshida, Y., Machida, T., Matsueda, H., and Sawa, Y.: Comparisons between XCH_4 from GOSAT Shortwave and Thermal Infrared Spectra and Aircraft CH_4 Measurements over Guam, SOLA, 8, 145–149, 2012.

Sawa, Y., Machida, T., and Matsueda, H.: Aircraft observation of the seasonal variation in the transport of CO_2 in the upper atmosphere, J. Geophys. Res., 117, D05305, doi:10.1029/2011JD016933, 2012.

Strow, L. L. and Hannon, S. E.: A 4-year zonal climatology of lower tropospheric CO_2 derived from ocean-only Atmospheric Infrared Sounder observations, J. Geophys. Res., 113, D18302, doi:10.1029/2007JD009713, 2008.

Takagi, H., Houweling, S., Andres, R. J., Belikov, D., Bril, A., Boesch, H., Butz, A., Guerlet, S., Hasekamp, O., Maksyutov, S., Morino, I., Oda, T., O'Dell, C. W., Oshchepkov, S., Parker, R., Saito, M., Uchino, O., Yokota, T., Yoshida, Y., and Valsala, V.: Influence of differences in current GOSAT XCO_2 retrievals on surface flux estimation, Geophys. Res. Lett., 41, 2598–2605, 2014.

Yokota, T., Yoshida, Y., Eguchi, N., Ota, Y., Tanaka, T., Watanabe, H., and Maksyutov, S.: Global Concentrations of CO_2 and CH_4 Retrieved from GOSAT: First Preliminary Results, SOLA, 5, 160–163, 2009.

Yoshida, Y., Ota, Y., Eguchi, N., Kikuchi, N., Nobuta, K., Tran, H., Morino, I., and Yokota, T.: Retrieval algorithm for CO_2 and CH_4 column abundances from short-wavelength infrared spectral observations by the Greenhouse gases observing satellite, Atmos. Meas. Tech., 4, 717–734, doi:10.5194/amt-4-717-2011, 2011.

Yoshida, Y., Kikuchi, N., Morino, I., Uchino, O., Oshchepkov, S., Bril, A., Saeki, T., Schutgens, N., Toon, G. C., Wunch, D., Roehl,

C. M., Wennberg, P. O., Griffith, D. W. T., Deutscher, N. M., Warneke, T., Notholt, J., Robinson, J., Sherlock, V., Connor, B., Rettinger, M., Sussmann, R., Ahonen, P., Heikkinen, P., Kyrö, E., Mendonca, J., Strong, K., Hase, F., Dohe, S., and Yokota, T.: Improvement of the retrieval algorithm for GOSAT SWIR XCO_2 and XCH_4 and their validation using TCCON data, Atmos. Meas. Tech., 6, 1533–1547, doi:10.5194/amt-6-1533-2013, 2013.